Characterization of highly crystalline lead iodide nanosheets prepared by room-temperature solution processing

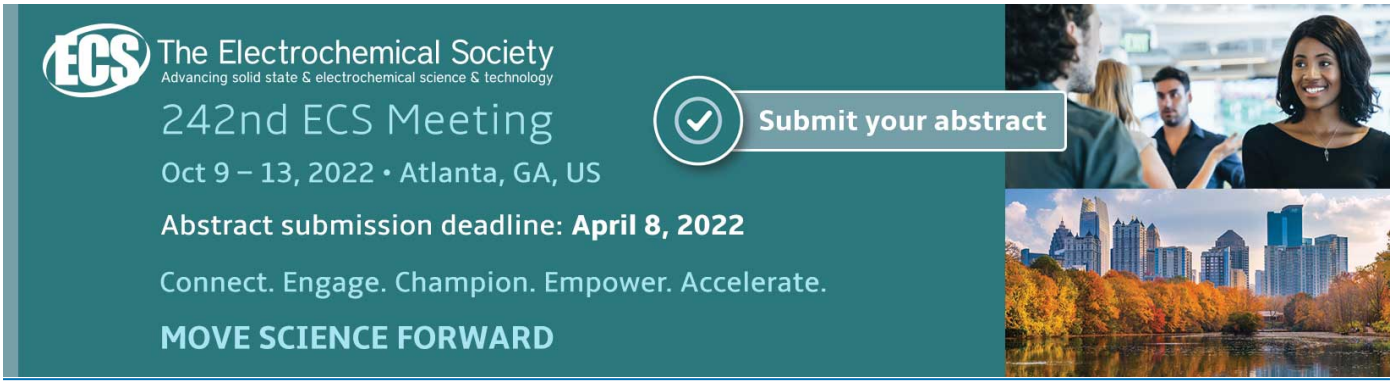

IOP Publishing Nanotechnology

Nanotechnology **28** (2017) 455703 (11pp) https://doi.org/10.1088/1361-6528/aa8e5c

Characterization of highly crystalline lead iodide nanosheets prepared by room-temperature solution processing

Riccardo Frisenda[1,8], Joshua O Island[2,9], Jose L Lado[3], Emerson Giovanelli[1], Patricia Gant[1], Philipp Nagler[4], Sebastian Bange[4], John M Lupton[4], Christian Schüller[4], Aday J Molina-Mendoza[5,10], Lucia Aballe[6], Michael Foerster[6], Tobias Korn[4], Miguel Angel Niño[1], David Perez de Lara[1], Emilio M Pérez[1], Joaquín Fernandéz-Rossier[3] and Andres Castellanos-Gomez[7,8]

[1] Instituto Madrileño de Estudios Avanzados en Nanociencia (IMDEA-Nanociencia), Campus de Cantoblanco, E-28049 Madrid, Spain
[2] Kavli Institute of Nanoscience, Delft University of Technology, Lorentzweg 1, 2628 CJ Delft, The Netherlands
[3] International Iberian Nanotechnology Laboratory (INL), Av. Mestre Jose Veiga, 4715-330, Braga, Portugal
[4] Department of Physics, University of Regensburg, Universitätsstrasse, Regensburg D-93040, Germany
[5] Departamento de Física de la Materia Condensada, Universidad Autónoma de Madrid, Campus de Cantoblanco, E-28049, Madrid, Spain
[6] ALBA Synchrotron Light Facility, Carrer de la Llum 2-26, Cerdanyola del Vallés, Barcelona E-08290, Spain
[7] Instituto de Ciencia de Materiales de Madrid (ICMM-CSIC), Campus de Cantoblanco, E-28049 Madrid, Spain

E-mail: riccardo.frisenda@imdea.org and andres.castellanos@csic.es

Received 4 July 2017, revised 20 September 2017
Accepted for publication 22 September 2017
Published 16 October 2017

Abstract

Two-dimensional (2D) semiconducting materials are particularly appealing for many applications. Although theory predicts a large number of 2D materials, experimentally only a few of these materials have been identified and characterized comprehensively in the ultrathin limit. Lead iodide, which belongs to the transition metal halides family and has a direct bandgap in the visible spectrum, has been known for a long time and has been well characterized in its bulk form. Nevertheless, studies of this material in the nanometer thickness regime are rather scarce. In this article we demonstrate an easy way to synthesize ultrathin, highly crystalline flakes of PbI_2 by precipitation from a solution in water. We thoroughly characterize the produced thin flakes with different techniques ranging from optical and Raman spectroscopy to temperature-dependent photoluminescence and electron microscopy. We compare the results to *ab initio* calculations of the band structure of the material. Finally, we fabricate photodetectors based on PbI_2 and study their optoelectronic properties.

Supplementary material for this article is available online

[8] Authors to whom any correspondence should be addressed.
[9] Present address: Department of Physics, University of California, Santa Barbara CA 93106, United States of America.
[10] Present address: Institute of Photonics, Vienna University of Technology, Gusshausstrasse 27-29, A-1040 Vienna, Austria.

Keywords: two-dimensional materials, PbI_2, lead iodide, transition metal halides, optoelectronics, *ab initio* calculations, direct bandgap

(Some figures may appear in colour only in the online journal)

Introduction

Shortly after the discovery of graphene by mechanical exfoliation, other two-dimensional (2D) materials were also isolated using the same approach [1, 2]. Among the different isolated 2D materials, the family of 2D semiconductors is especially relevant for applications as their intrinsic bandgap makes them suitable for different electronic and optoelectronic devices [3, 4]. Although theory predicts a large number of 2D semiconductors that can be produced by mechanical exfoliation (>1000) [5–9], so far the number of compounds that have been experimentally studied is rather limited (<20) [10–12]. The chalcogenides group, and in particular the transition metal dichalcogenides (TMDC) such as molybdenite (MoS_2), is probably the most investigated family of 2D materials [13, 14]. The transition metal halides (TMH) family, on the other hand, is a scarcely explored family of materials in the few-layer limit, although it contains many examples of layered materials [15–18]. In their bulk form, lead-based TMHs are gaining a great deal of attention as they can be used as a source to synthesize metal halide perovskite solar cells [19–21]. Moreover, ultrathin TMHs present several characteristics that make them an interesting complement to TMDCs, such as their direct bandgap in multilayer samples and the absolute value of the bandgap that spans a range not covered by the TMDCs.

In this study, we use solution-based synthesis of lead iodide (PbI_2) followed by mechanical exfoliation to produce thin flakes. We study the isolated layers by micro-reflectance and transmission spectroscopy, atomic force microscopy (AFM), transmission electron microscopy (TEM), Raman spectroscopy, micro x-ray photoemission spectroscopy, temperature-dependent photoluminescence (PL) spectroscopy and photocurrent spectroscopy. To complement the material characterization we perform *ab initio* calculations of the thickness dependency of the PbI_2 band structure. Even though many methods have been demonstrated to synthesize PbI_2 [22], such as the Bridgman method, solution processing and vapor deposition studies of this material are still rather scarce [23]. Our results demonstrate that crystalline large-area ultrathin lead iodide flakes can be easily synthesized at room temperature from an aqueous solution.

Results and discussions

Lead iodide is a layered material, belonging to the TMHs family, which has been studied in applications such as source for perovskite solar cells [19], photodetectors [24] and nuclear radiation detectors [25]. Its structure, schematically depicted in figure 1(a) for a single-layer, is formed by covalently bonded I and Pb atoms arranged in an in-plane hexagonal lattice with out-of-plane van der Waals interactions between the different layers [26]. In order to gain insight into the expected material electronic properties, we computed the band structure based on the crystal structure described above (see computational methods section in the supplementary information is available online at stacks.iop.org/NANO/28/455703/mmedia). Figure 1(b) shows the band structure calculated for a PbI_2 single-layer (left) and for a bulk crystal (right). When going from bulk to a single-layer the nature of the bandgap changes, passing from direct in bulk (with a value of 2.26 eV) to indirect in the monolayer (2.64 eV). The magnitude of the direct gap increases monotonically when thinning down the material from a bulk crystal to a single-layer, as can be seen in figure 1(c) and the crossover from a direct to an indirect bandgap happens between one and two layers, in agreement with literature [27].

Thin PbI_2 crystals, with lateral dimensions of up to approximately 100 μm and thicknesses ranging from a few nanometers up to hundreds of nanometers, can be synthesized with a simple precipitation process [23]. We use as a starting material PbI_2 in powder (99% purity, Sigma-Aldrich). The solubility of PbI_2 in water strongly depends on the temperature in the range between 20 °C and 100 °C, with PbI_2 being more soluble in hot water (4.1 g l^{-1} at 100 °C) than in cold water (0.8 g l^{-1} at 20 °C) [28, 29]. Panels 1 and 2 of figure 2(a) show a vial containing a supersaturated solution of PbI_2 powder (≈0.1 g) in Milli-Q water (20 ml) respectively at 25 °C and at 100 °C. The change in solubility of PbI_2 is reflected by the change in the color of the liquid. During the cooling down of the solution, dissolved Pb and I species start to aggregate and form crystals of PbI_2, which appear as a fine dust in panels 3–5 of figure 2(a) (see the comparison between the top and bottom rightmost panels in figure 2(a)). To isolate the PbI_2 nanosheets, a 1 ml droplet of the saturated PbI_2 solution at 100 °C is drop-cast onto the surface of a polydimethylsiloxane (PDMS) stamp. When the drop cools down, PbI_2 crystals of various sizes and thicknesses grow, as shown in the optical micrographs recorded at different times shown in figure 2(b). The crystallization process can last from a few seconds to several minutes and by monitoring the process with a microscope (20× magnification, working distance of 20.5 mm) we can draw up the liquid at the desired time from the PDMS surface with a pipette in order to reach the desired density of crystals on the PDMS. The advantage of this method is that the as-produced crystals can be readily transferred to another substrate or onto pre-patterned nanoscale structures using the deterministic transfer method [30]. Moreover, thinner flakes can be achieved by mechanical exfoliation of the as-crystallized flakes with another PDMS stamp. The crystallization process is reproducible and gives rise to PbI_2 crystallites with hexagonal shape (see supplementary information), consistent with previous studies using different PbI_2 syntheses [27, 31, 32].

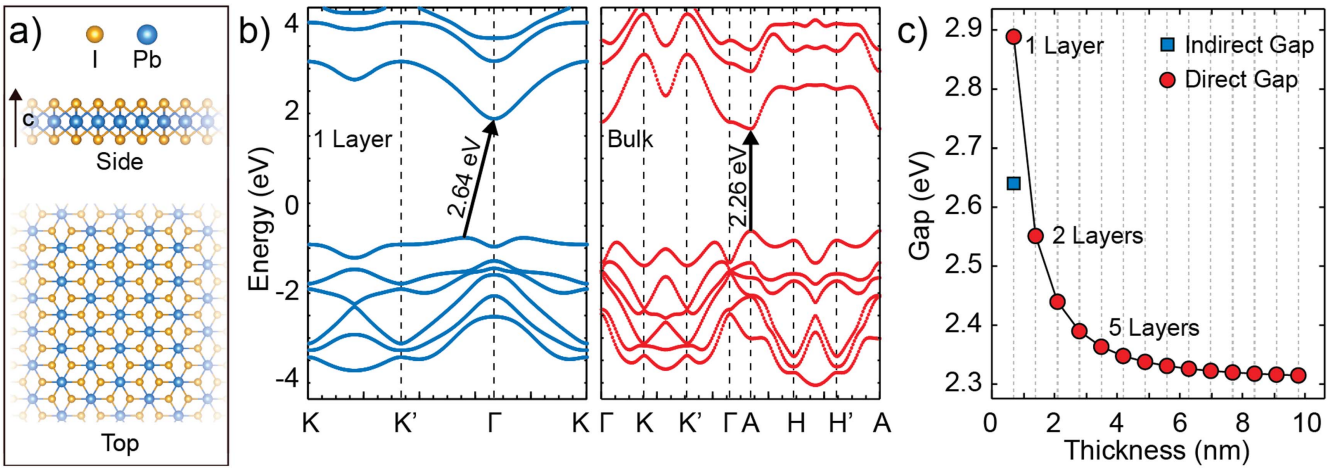

Figure 1. (a) Crystal structure of a single-layer PbI_2. The blue balls are lead (Pb) atoms and the orange balls represent iodine (I) atoms. (b) Band structure of a PbI_2 single-layer (left) and bulk (right). (c) Calculated bandgap energy of PbI_2 as a function of the thickness.

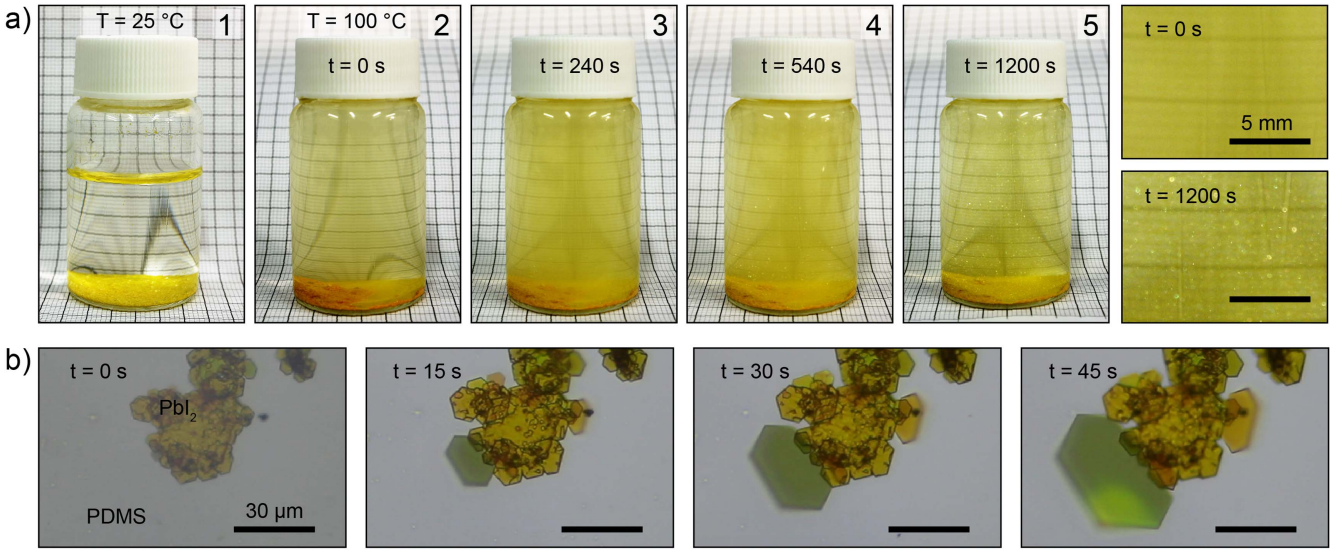

Figure 2. (a) Time sequence of the steps of the synthesis of PbI_2 crystallites from solution. First, PbI_2 in powder is added to Milli-Q water at 25 °C (1) and heated to 100 °C (2). When the hot solution cools down crystallites of PbI_2 form and appear as a fine dust (3–5). The last two panels on the right are zoomed views of the solution from steps 2 and 5. (b) Microscope pictures taken at different times of the formation of a PbI_2 thin crystal from a drop deposited on a PDMS substrate.

To relate the thickness of the PbI_2 crystals to the optical properties of the material we first characterized the PbI_2 flakes by a combination of optical and AFM. Figures 3(a)–(e) show optical micrographs of different flakes that have been transferred onto a SiO_2/Si substrate with 285 nm oxide. Similar to the case of graphene and other 2D materials, different flakes deposited on SiO_2/Si present different colors according to their thickness because of thin-film interference effects [33]. We have used AFM measurements to accurately determine the thickness of the flakes in figure 3. From comparison of the AFM data to the microscope pictures we extract a calibration chart, shown in figure 3(f), which can be used to estimate the thickness of PbI_2 flakes from their color at first glance. More quantitative information can be obtained from the analysis of the red/green/blue channels of the optical images. Figure 3(g) shows the optical contrast of the PbI_2 flakes on SiO_2 calculated for different flakes from the intensity of the red/green/blue channels according to $C = (I_{R,flake} - I_{R,sub})/(I_{R,flake} + I_{R,sub})$, where C is the optical contrast and $I_{R,flake}$ ($I_{R,sub}$) is the intensity of the light reflected by the PbI_2 flake (substrate). When the contrast is zero the flake is not detectable, while when the contrast is positive (negative) the flake appears brighter (darker) than the substrate. In all the three channels the optical contrast of PbI_2 flakes does not present a monotonic dependence on the thickness, but instead it shows oscillations and it explores both positive and negative values because of thin film interference effects. Notice that the PbI_2 flakes in panels (d), (e) and (g) of figure 3 have been mechanically exfoliated from thicker flakes.

Another simple method that is used to estimate the thickness of ultra-thin 2D materials is the analysis of a photograph of the flake under study deposited on a transparent substrate and recorded in transmission illumination mode with a white light source. The inset of figure 3(h) shows

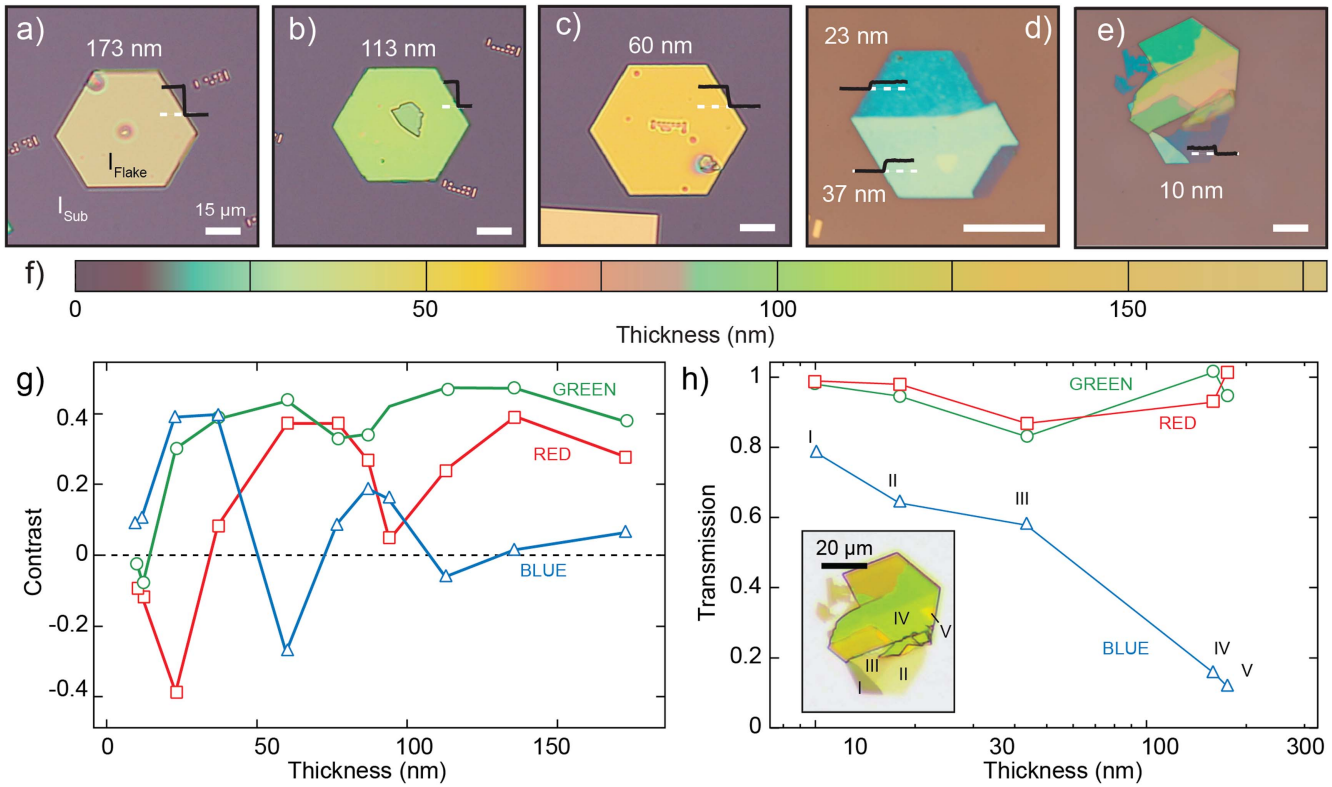

Figure 3. (a)–(e) Optical image of a PbI_2 flake transferred onto a 285 nm SiO_2/Si substrate. The black line is the topographic profile measured with an AFM to extract the flake thickness. (f) Color chart for thickness calibration of PbI_2 flakes on SiO_2/Si. (l) Optical contrast of the flakes as a function of the thickness calculated from the red, green and blue channels of panels (a)–(e). (h) Transmission of PbI_2 on PDMS as a function of the flake thickness. Inset: optical micrograph of a PbI_2 flake showing various regions of different thickness recorded in transmission illumination mode (white light source). The roman numerals indicate the regions of the flake used to extract the transmission and the thickness data.

a microscope picture of a PbI_2 flake on PDMS illuminated in transmission mode. Different colors and shades correspond to different values of thickness. We extract the transmission, $T = I_{T,flake}/I_{T,sub}$, for red/green/blue channels at five different points on the flake. After recording the transmission illumination mode microscope optical photograph we transfer the flake onto a SiO_2/Si substrate to perform AFM measurements and extract the thickness of the flake. Figure 3(h) shows the local transmission of the flake as a function of the thickness for red/green/blue channels. Due to the large band gap of the PbI_2, the transmission of the flakes remains close to unity in the red and green channels even for thicker flakes. By contrast, the transmission extracted from the blue channel shows a monotonic dependence on the thickness and it can be used to have a rough and quick estimation of the thickness of ultra-thin PbI_2 crystals.

To extract more quantitative information about the optical properties of PbI_2 we study the thickness dependence of the optical contrast of PbI_2 on SiO_2/Si resolved in energy. To this end, we employ a micro-reflectance spectroscopy set-up that was previously described elsewhere [34, 35]. Briefly, the flakes are illuminated in normal incidence with the white light produced by a tungsten halogen lamp, and the reflected light is collected with an optical fiber (core diameter of 105 μm), which acts as a confocal pinhole, placed at the image plane of the trinocular of an optical microscope. The other end of the fiber optic cable is connected to a compact charge-coupled device (CCD) spectrometer (Thorlabs), allowing to measure the spectrum of the reflected light from 400–900 nm with ≈1 nm resolution. By measuring the reflectance spectrum of the bare substrate (SiO_2/Si) and that of the PbI_2 flake, we can determine the optical contrast C in a broad range of the visible and near-infrared part of the electromagnetic spectrum. Figure 4(a) shows the optical contrast spectra recorded for four flakes with different thickness. A comparison of the different spectra shows that the largest positive contrast can be achieved at a wavelength of ≈550 nm, independent of the PbI_2 thickness. At longer wavelengths the optical contrast spectra reverse their sign, going from positive to negative, and present a dip with the largest negative contrast at a wavelength in the range between 600 and 800 nm depending on the thickness of PbI_2. Figure 4(b) shows the optical contrast as a function of the PbI_2 thickness, extracted at different wavelengths between 450 and 700 nm. The contrast data have an oscillatory behavior with a larger period for longer wavelengths, which can be well fit to the Fresnel equation represented by dashed lines in figure 4(b) [33]. From each spectrum taken at a certain wavelength λ, we extract the complex refractive index at that wavelength $\underline{n}(\lambda)$.

From the Fresnel equation fit of figure 4(b), by fitting hundreds of curves with different wavelengths between 400 and 800 nm, we calculate the wavelength-resolved PbI_2 complex refractive index $\underline{n} = n - i\kappa$. Figure 5(a) shows the refractive index n and the extinction coefficient κ of PbI_2 as a

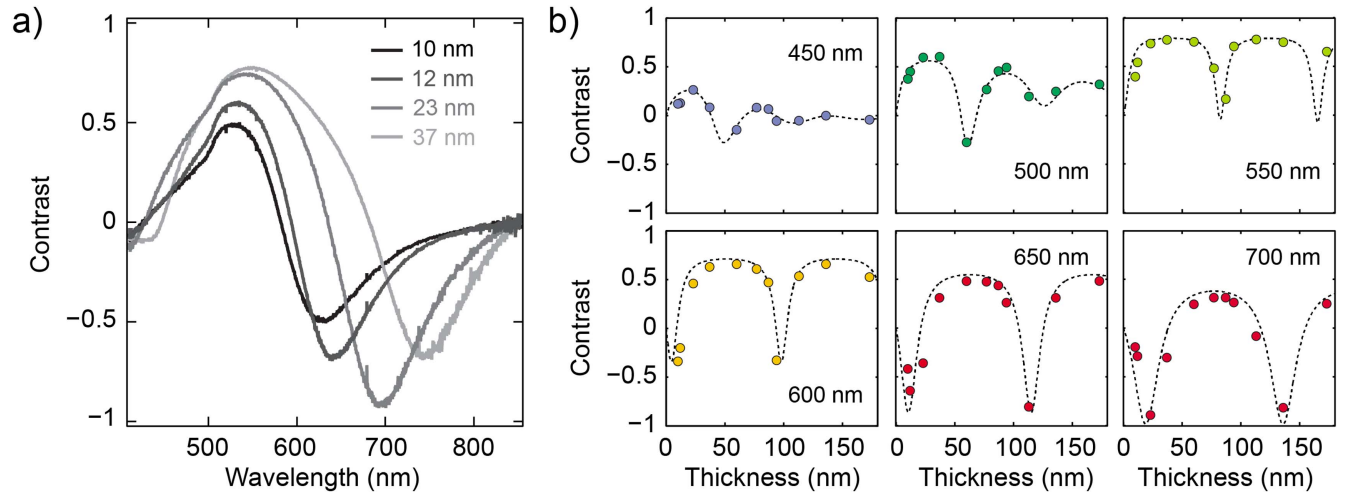

Figure 4. (a) Wavelength-resolved optical contrast of PbI_2 flakes of different thickness. (b) Optical contrast as a function of thickness extracted at different wavelengths. The dashed lines are fits to the Fresnel equation.

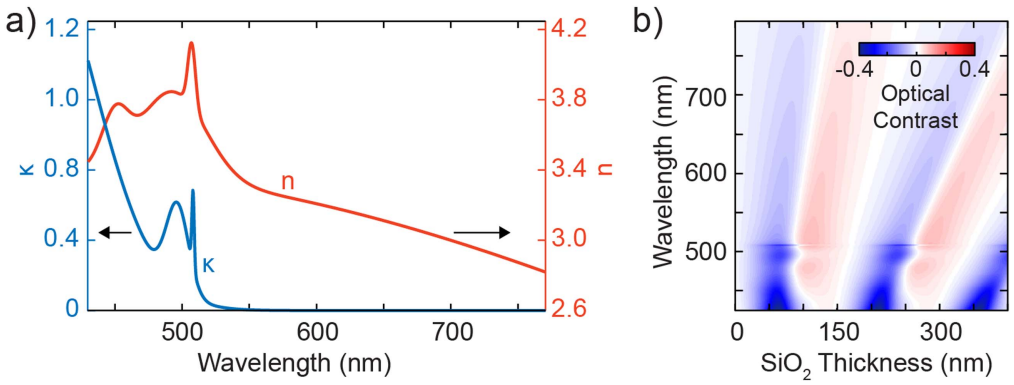

Figure 5. (a) Real (n) and imaginary (κ) components of the refractive index ($\underline{n} = n - i\kappa$) calculated from the fits of figure 4(b). (b) Calculated optical contrast as a function of the illumination wavelength and SiO_2 thickness for PbI_2 on a SiO_2/Si substrate.

function of the wavelength. The refractive index is a slowly varying function of the wavelength while the extinction coefficient, which is related to the absorption, shows sharper features. For wavelengths longer than 510 nm, κ takes values close to zero, indicating that the material does not absorb at these wavelengths. On the other hand, at wavelengths shorter than 510 nm the extinction coefficient steadily increases, which is due to direct band-to-band transitions. Finally, we use the estimated complex refractive index to calculate the optical properties of a thin film of PbI_2 under normal incidence using the Fresnel equation. Figure 5(b) displays a colormap that represents the calculated optical contrast C of a monolayer PbI_2 as a function of the illumination wavelength and the thickness of the SiO_2 dielectric layer. For a given excitation wavelength, the contrast oscillates around zero with a period that increases with the wavelength of the incident light. The maximum contrast is achieved for SiO_2 thicknesses of approximately 70, 220 and 350 nm. Notice that the abrupt change in the colormap around 510 nm is due to a change in the magnitude of the optical contrast caused by the strong absorption of PbI_2 at the bandgap (see the graph of κ versus wavelength).

Raman spectroscopy, which has been demonstrated to be a very powerful tool to characterize the quality and the thickness of 2D materials [36, 37], was employed to characterize the flakes previously studied in figures 3 and 4. Figure 6(a) shows the Raman spectra collected for flakes 23–180 nm thick whose intensities are all normalized by the intensity of the peak at 520 cm^{-1}, arising from transverse optical modes of the Si substrate. The excitation wavelength is 532 nm (2.33 eV), which is close to resonance with the fundamental absorption band (≈2.3 eV). The spectra show an intense and broad peak centered at approximately 214 cm^{-1} that is characteristic of the $A_1{}^2$ vibrational mode of hexagonal PbI_2 and is indicative of the crystallinity of the sample [38–40]. The intensity of this peak increases with the PbI_2 thickness and can be used to estimate the thickness of the material without the need of topographic measurements. Figure 6(b) shows the ratio between the $A_1{}^2$ peak and the Si 520 cm^{-1} peak as a function of the PbI_2 thickness. Due to the strong background in the Raman spectra we cannot access the energy range below 150 cm^{-1} which contains additional Raman peaks of PbI_2 that are sensitive to the crystalline phase of the material [41, 42].

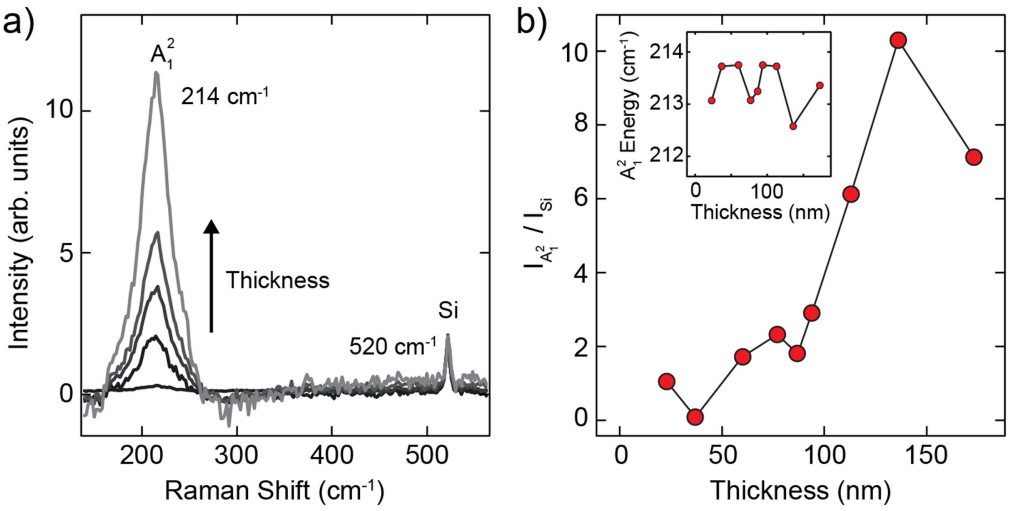

Figure 6. (a) Raman spectra of PbI_2 flakes with different thickness recorded with an excitation wavelength of 532 nm. All the spectra have been normalized by the intensity of the Si peak at 520 cm^{-1}. (b) Ratio between the intensities of the A^1_2 PbI_2 peak (214 cm^{-1}) and the Si peak (520 cm^{-1}) as a function of the PbI_2 thickness. Inset: center of the A^1_2 peak as a function of PbI_2 thickness.

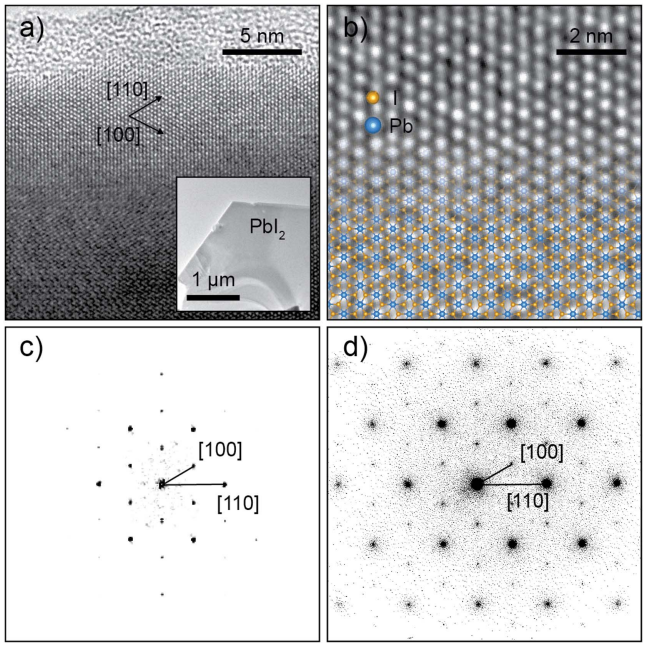

Figure 7. (a) High-resolution transmission electron microscopy (TEM) image of a PbI_2 thin flake. Inset: low magnification TEM image of the flake. (b) Zoom in the TEM image of panel (a). Superimposed to the TEM image there is a sketch of 2H-PbI_2 crystal lattice. Lead atoms are represented in blue and iodine in orange. (c) Two-dimensional Fourier transform of the TEM image of panel (b). (d) Selected area electron diffraction of the PbI_2 flake.

To characterize the crystal structure of the fabricated PbI_2 flakes we study them with high-resolution TEM. The samples are fabricated by simply drop casting the saturated hot solution of PbI_2 and water onto a nickel TEM grid with 6 μm holes, which leads to crystallization of thin hexagonal flakes covering a few holes. Figure 7(a) shows a high-resolution TEM image (20 nm × 20 nm) of a PbI_2 flake where individual Pb atoms are visible and in the inset a low-magnification image (3 μm × 3 μm) of the same flake is shown. To better analyze the atomic arrangement we show a zoom of the TEM image in figure 7(b) where we superimposed a drawing of the PbI_2 lattice in the 2H polytype. We find a perfect match between the atomic arrangements in the TEM image and the PbI_2 2H polytype generated lattice, which is in agreement with the minimum energy structure found in the *ab initio* calculations and with previous studies with similar synthesis [26, 43]. Notice that because of differences in the notation, the 2H polytype in PbI_2 is identical in stacking to the 1T polytype in TMDC such as MoS_2 or WSe_2 [44].

Additionally, using a Matlab algorithm we extract the distance between all the pairs of prime- and second-nearest neighbor atoms in figure 7(a) (see the supplementary information). We find an average distance of (2.65 ± 0.03) Å for the nearest neighbors, which is consistent with the lead–lead distance and corresponds to the lattice spacing of the (100) planes. The second-nearest neighbor pairs of atoms have an average distance of (4.56 ± 0.02) Å which matches perfectly the lattice constant of PbI_2 [15]. The 2D Fourier transform of the TEM image, shown in figure 7(c), reveals the long-range order of the imaged lattice. Finally, the clear diffraction spots of the electron diffraction image of figure 7(d) are consistent with the single-crystalline nature and long-range order of the fabricated PbI_2 flakes.

We also perform micro-XPS and low-energy electron microscopy measurements of PbI_2 crystallites transferred onto a platinum substrate. The results, discussed in the supplementary information, indicate a steady desorption of iodine with time when the sample is placed in ultrahigh vacuum (10^{-10} mbar) and under x-ray irradiation. We observe a full desorption of the iodine atoms when the samples were annealed at temperatures larger than 150 °C in ultrahigh vacuum conditions.

After establishing the crystallinity of the PbI_2 ultra-thin crystals, we investigate their optical properties with temperature-dependent PL measurements. The PbI_2 flakes grown from solution on PDMS are deterministically transferred onto

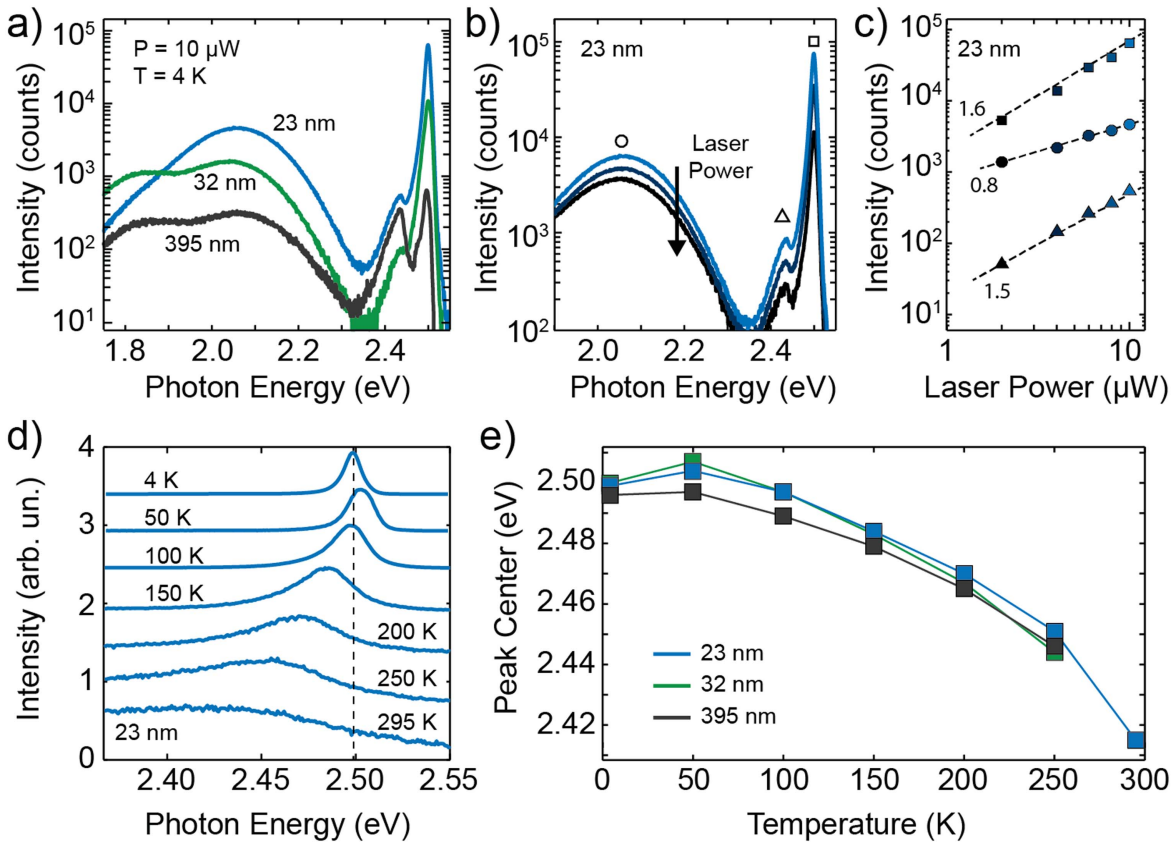

Figure 8. (a) Photoluminescence spectra of three different PbI_2 flakes on SiO_2/Si with an excitation wavelength of 375 nm and power of 10 μW. (c) Log–log plot of the intensity of the photoluminescence peaks at 2.49 eV (squares), 2.42 eV (triangles) and 2.05 eV (circles) as a function of laser excitation power for the 23 nm thick flake. The numbers indicate the exponent of a power law fit performed on each curve (a value of 1 indicates a linear dependence). (d) Photoluminescence spectra of a 23 nm thick PbI_2 flake recorded at different temperatures from 4 to 295 K. (e) Energy of the highest-energy photoluminescence peak as a function of temperature.

a SiO_2/Si substrate and subsequently studied in a self-built micro-PL system, details are published elsewhere [45]. Briefly, a continuous-wave laser (central wavelength 375 nm) is coupled into a 100× microscope objective and focused to a sub-micron spot on the sample, which is mounted in a He-flow cryostat. The PL emission from the sample is collected by the same microscope objective and coupled into a spectrometer with a Peltier-cooled CCD sensor.

In figure 8(a) we plot the PL spectra of three different flakes with thickness from 23 to 395 nm in a semi-logarithmic representation recorded at 4 K and with the same excitation power of 10 μW (see the supplementary information for optical pictures of the flakes). The spectra present common features, starting from high energy we find a peak centered at 2.49 eV. The 395 nm thick flake shows a shoulder on the low-energy side of the first peak. Additionally, in all three spectra a weaker peak is present at 2.42 eV and a broad peak or double peak is centered at lower energies between 2.1 and 1.8 eV. The peak at 2.49 eV is the fundamental excitonic peak due to direct band-to-band transition, and its energy is in good agreement with the onset of absorption observed in the refractive index data discussed above [46, 47]. We note that all flakes investigated in the PL measurements are so thick that neither changes of the band structure nor exciton confinement effects which would shift the transition energies are to be expected. Remarkably, we observe that the thinnest flake (23 nm) shows the highest PL intensity. The peak at 2.42 eV can be interpreted as due to bound exciton by a comparison with literature [40]. On the other hand, the lowest peak at 2.05 eV, which is called G band, does not have an excitonic origin, but is due to defects in the surface of the PbI_2 samples and especially to the presence of Pb^+ ions [40, 42]. Figure 8(b) shows the PL spectra of the 23 nm thick flake recorded at different excitation powers. We extract the intensity of the free and bound excitonic peaks and of the G band for different laser powers and figure 8(c) shows the results for the 23 nm thick flake. From the log–log plot one can see that for all the peaks the emission intensity I displays a power-law dependence on the excitation power, which can be described by the formula $I \approx P^k$. The dependency of the PL intensity on the laser power is an indicator of the nature of the different recombination processes. The intensity of the peaks at 2.49 and 2.42 eV can be fit with exponents $k = 1.6$ and 1.5 respectively, indicating a super-linear scaling of I versus P. By contrast, the G band intensity scales sub-linearly with the excitation power with exponent $k = 0.8$. According to literature, a value of k in the range between 1 and 2 is related to exciton-like transitions while a value of k smaller than 1 is related to recombination of trapped with free carriers [48, 49], confirming that the G band is due to defects in the

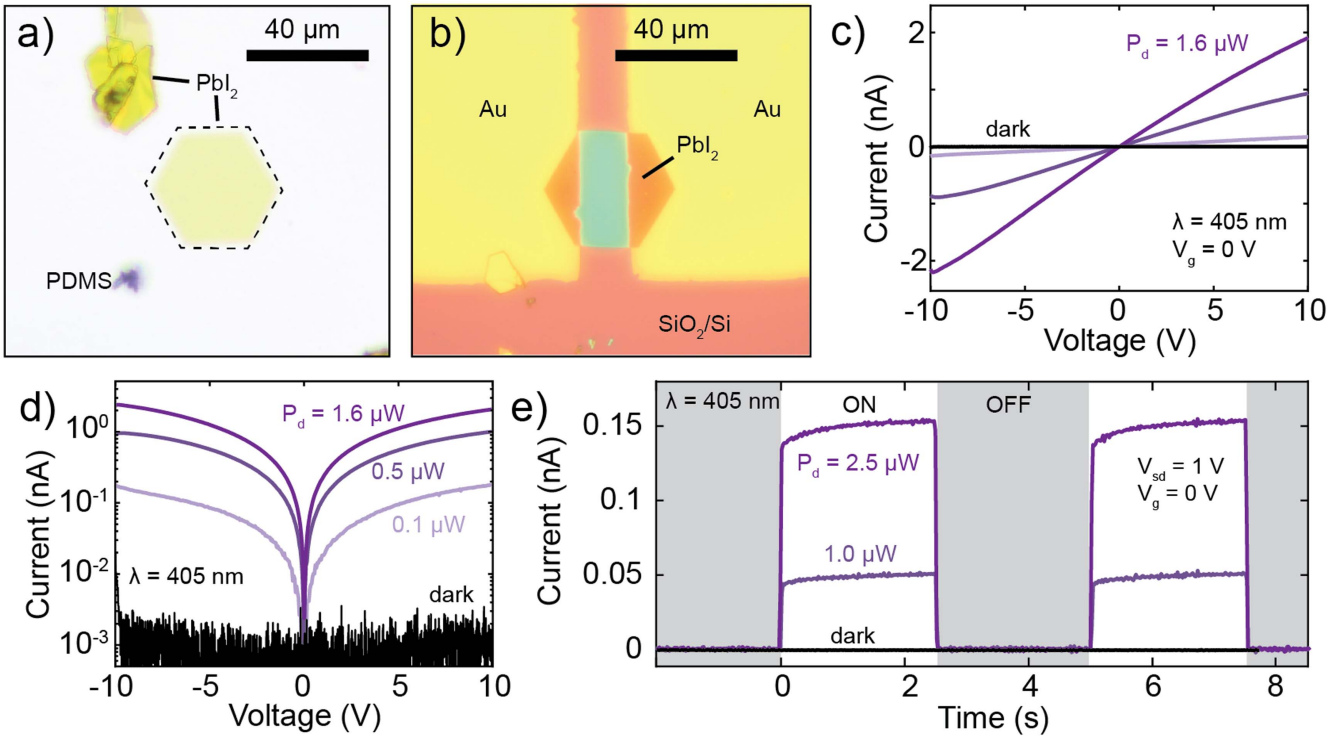

Figure 9. (a) Microscope picture of a PbI_2 flake on PDMS in transmission illumination mode. The dashed line highlights the PbI_2 flake used to fabricate the field effect transistor. (b) Optical picture of the same flake shown in panel (a) after being transferred between two Au electrodes. (c) Current versus source–drain voltage characteristics of the device in dark and under illumination with a 405 nm LED and different powers. (d) Semi-logarithmic representations of the IV_{SD} curves of panel (c). Notice that the sign of the current at negative bias has been reversed. (e) Current versus time at fixed bias voltage in dark (black curve) and under modulated illumination (violet curves).

crystal structure and that the higher energy peaks are due to excitonic transitions.

We also investigate the temperature dependence of the PL emission. Figure 8(d) shows the PL spectra of a 23 nm thick PbI_2 flake recorded between 4 and 295 K. Between 4 and 50 K, we observe a slight blueshift for the 23 and 32 nm thick flakes (see figure 8(e)), indicative of a de-trapping of excitons bound to shallow defects such as charged surface adsorbates. As the temperature is increased further, the main excitonic peak shows an energetic redshift and its intensity decreases. This temperature dependence of the excitonic peak reflects the thermally induced change in the bandgap of PbI_2 and the graph of the excitonic peak center versus temperature of figure 8(e) can be fit to the Bose–Einstein model, see supplementary information.

Finally, we study the optoelectronic properties of thin PbI_2 flakes by fabricating photodetector devices. In total we fabricated five PbI_2-based photodetectors, four of which were fabricated on a SiO_2/Si substrate while one on a transparent and flexible polycarbonate substrate (see section 6 of the supplementary information). We transfer a 15 nm thick PbI_2 flake from a PDMS substrate, see figure 9(A), bridging drain and source Au electrodes pre-patterned on a SiO_2/Si substrate (see supplementary information for the AFM profile of the flake). The Si is heavily doped in order to use it as a back gate electrode and in the measurements discussed below it is kept at zero voltage. An optical picture of the final device is shown in figure 9(b). We record current versus drain–source voltage (IV_{SD}) characteristics of the device in dark and under illumination. We use various high-power LEDs, with central wavelengths ranging from 375 to 1050 nm, that are focused on the surface of PbI_2 on spot diameter of 200 μm providing a homogenous illumination over the entire device area. Figure 9(c) shows IV_{SD} characteristics acquired in dark and under illumination using a 405 nm LED with increasing optical power. The optical power indicated in the plots, P_D, is the power of the radiation falling on the device, calculated by dividing the total beam power by the spot area and multiplying the result for the area of the PbI_2 transistor channel (684 μm^2) estimated from the microscope picture. The photocurrent (difference between the current upon illumination and in dark) generated in the device displays a sub-linear dependence on the incident power (exponent equal to 0.7, see supporting information) which suggests the influence of defects in the dynamics of the charge carriers [50–52]. The semi-logarithmic representation of the IV_{SD} of figure 9(d) reveals an on–off ratio larger than 2000 for the largest optical power.

We also study the time response of the device by recording the current at a fixed source–drain voltage as a function of time (It) while modulating the light intensity with a ≈0.5 Hz square wave. Figure 9(e) report the current at $V_{SD} = 1$ V in dark and under modulated illumination. We cannot directly resolve the switching times of the device when the illumination is turned on or off with our experimental time resolution. Instead, we can define an upper boundary of 20 ms

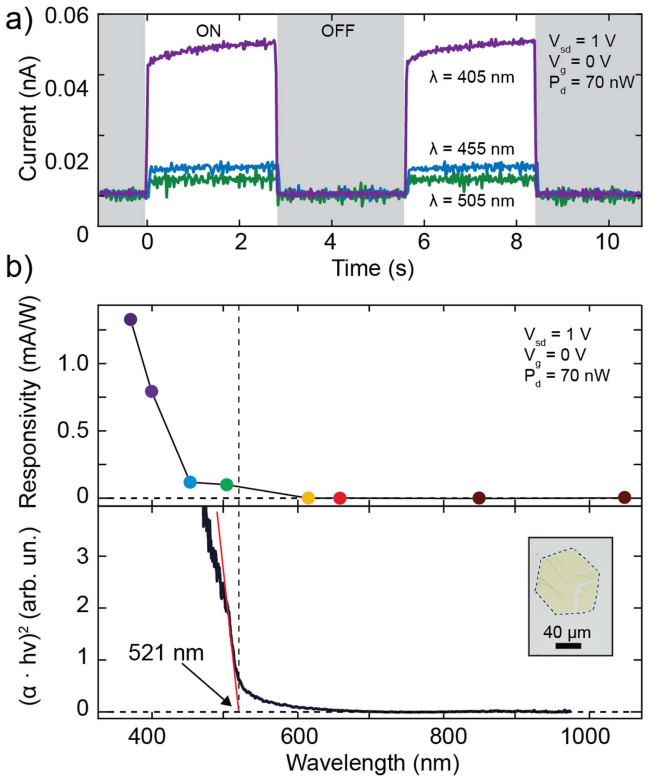

Figure 10. (a) Current versus time at fixed bias voltage under modulated illumination with different wavelengths and same optical power. (b) Top: responsivity of the PbI_2 device for different wavelengths. Bottom: Tauc plot with exponent 2 (direct gap) of the absorbance of the PbI_2 shown in the inset, extracted from transmittance measurements. The red line is a linear fit to the data and the energy at which it intersects the *x*-axis is the estimated bandgap.

for the device switching time. By recording *It* traces with different excitation wavelength all set at the same optical power we can study the energy dependence of the PbI_2 responsivity. Figure 10(a) shows three *It* traces recorded at wavelengths $\lambda = 405$, 455 and 505 nm. The device displays the same fast response to all the wavelengths and has the largest response for the shortest wavelength. We extract the photocurrent generated at each wavelength $I_{Ph}(\lambda)$ in the on state and we calculate the responsivity according to $R(\lambda) = I_{Ph}(\lambda)/P_D$. In the top panel of figure 10(b) we plot the responsivity extracted from the *It* traces as a function of excitation wavelength. The responsivity is zero for wavelengths larger than 505 nm and it steadily increases at shorter wavelengths with the largest value recorded equal to 1.3×10^{-3} A W^{-1}, which is a low value compared to other multilayer 2D materials [52]. The behavior of the responsivity is consistent with the bandgap of PbI_2 of 2.38 eV, corresponding to a wavelength of 521 nm, extracted from the Tauc plot of the absorbance (with Tauc exponent for a direct gap) shown in the bottom panel of figure 10(b) [32]. The different photodetectors built from PbI_2 and shown in the supplementary information have comparable responsivities to the main text device.

Conclusions

In conclusion, we have discussed an easy route to synthesize highly crystalline nanosheets of PbI_2 from an aqueous solution and we presented a thorough characterization of the resulting material. We studied the reflectance of PbI_2 as a function of the crystal thickness to extract the refractive index components n and κ of the material and found that the onset of absorption spectrally matches the main emission peak we observed in PL. Additionally, temperature- and power-dependent PL measurements revealed defect-related emission and a redshift of the main emission peak with increasing temperature due to a decreasing band gap. Raman spectroscopy, TEM and electron diffraction measurements demonstrated the crystallinity of the as-grown and exfoliated PbI_2 samples. Finally we fabricated photodetectors based on PbI_2 thin flakes and studied their optoelectronic properties. The experiments have been compared to *ab initio* calculations of the electronic band structure of the material.

Acknowledgments

We acknowledge financial support from the European Commission under the Graphene Flagship (CNECTICT-604391), and European Research Council (ERC-StG-MINT 307609), the MINECO, the Comunidad de Madrid, the Netherlands Organisation for Scientific Research (NWO), and the German Science Foundation (DFG). We are also grateful to B Galler and R Zeisel (OSRAM OS, Regensburg) for technical assistance in the photoluminescence experiments. JLL and JFR acknowledge financial support by Marie-Curie-ITN 607904-SPINOGRAPH. JFR acknowledges financial support from MEC-Spain (MAT2016-78625-C2).

Competing interests

The authors declare no competing financial interests.

Funding

ACG European Commission under the Graphene Flagship: contract CNECTICT-604391. ACG MINECO: Ramón y Cajal 2014 program RYC-2014-01406 ACG MINECO: program MAT2014-58399-JIN. ACG Comunidad de Madrid: MAD2D-CM program (S2013/MIT-3007). RF Netherlands Organisation for Scientific Research (NWO): Rubicon 680-50-1515. DPdL MINECO: program FIS2015-67367-C2-1-p. EMP European Research Council (ERC-StG-MINT 307609). EMP MINECO: CTQ2014-60541-P. EG AMAROUT II fellowship program: grant for transnational mobility (Marie Curie Action, FP7-PEOPLE-2011-COFUND (291803)). PN, TK: DFG: GRK 1570 and KO3612/1-1. JML: DFG SFB 689 JLL, JFR Marie-Curie-ITN 607904-SPINOGRAPH. JFR MINECO-Spain MAT2016-78625-C2. LA and MF: MINECO: MAT2015-64110-C2-2-P.

ORCID iDs

Riccardo Frisenda https://orcid.org/0000-0003-1728-7354
Emilio M Pérez https://orcid.org/0000-0002-8739-2777
Andres Castellanos-Gomez https://orcid.org/0000-0002-3384-3405

References

[1] Xu M, Liang T, Shi M and Chen H 2013 Graphene-like two-dimensional materials *Chem. Rev.* **113** 3766–98
[2] Butler S Z, Hollen S M, Cao L, Cui Y, Gupta J A, Gutierrez H R, Heinz T F, Hong S S, Huang J and Ismach A F 2013 Progress, challenges, and opportunities in two-dimensional materials beyond graphene *ACS Nano* **7** 2898–926
[3] Koppens F, Mueller T, Avouris P, Ferrari A, Vitiello M and Polini M 2014 Photodetectors based on graphene, other two-dimensional materials and hybrid systems *Nat. Nanotechnol.* **9** 780–93
[4] Radisavljevic B, Radenovic A, Brivio J, Giacometti V and Kis A 2011 Single-layer MoS_2 transistors *Nat. Nanotechnol.* **6** 147–50
[5] Ataca C, Şahin H and Ciraci S 2012 Stable, single-layer MX_2 transition-metal oxides and dichalcogenides in a honeycomb-like structure *J. Phys. Chem.* C **116** 8983–99
[6] Rasmussen F A and Thygesen K S 2015 Computational 2D materials database: electronic structure of transition-metal dichalcogenides and oxides *J. Phys. Chem.* C **119** 13169–83
[7] Lebègue S, Björkman T, Klintenberg M, Nieminen R M and Eriksson O 2013 Two-dimensional materials from data filtering and *ab initio* calculations *Phys. Rev.* X **3** 031002
[8] Miro P, Audiffred M and Heine T 2014 An atlas of two-dimensional materials *Chem. Soc. Rev.* **43** 6537–54
[9] Tang Q and Zhou Z 2013 Graphene-analogous low-dimensional materials *Prog. Mater. Sci.* **58** 1244–315
[10] Castellanos-Gomez A 2016 Why all the fuss about 2D semiconductors? *Nat. Photon.* **10** 202–4
[11] Schwierz F, Pezoldt J and Granzner R 2015 Two-dimensional materials and their prospects in transistor electronics *Nanoscale* **7** 8261–83
[12] Bhimanapati G R *et al* 2015 Recent advances in two-dimensional materials beyond graphene *ACS Nano* **9** 11509–39
[13] Splendiani A, Sun L, Zhang Y, Li T, Kim J, Chim C-Y, Galli G and Wang F 2010 Emerging Photoluminescence in Monolayer MoS_2 *Nano Lett.* **10** 1271–5
[14] Mak K F, Lee C, Hone J, Shan J and Heinz T F 2010 Atomically thin MoS_2: a new direct-gap semiconductor *Phys. Rev. Lett.* **105** 136805
[15] Pałosz B and Salje E 1989 Lattice parameters and spontaneous strain in AX_2 polytypes: CdI_2, PbI_2 SnS_2 and $SnSe_2$ *J. Appl. Crystallogr.* **22** 622–3
[16] Toulouse A S, Isaacoff B P, Shi G, Matuchová M, Kioupakis E and Merlin R 2015 Frenkel-like Wannier–Mott excitons in few-layer PbI_2 *Phys. Rev.* B **91** 165308
[17] Huang B, Clark G, Navarro-Moratalla E, Klein D R, Cheng R, Seyler K L, Zhong D, Schmidgall E, McGuire M A and Cobden D H 2017 Layer-dependent ferromagnetism in a van der Waals crystal down to the monolayer limit *Nature* **546** 270–3
[18] McGuire M 2017 Crystal and magnetic structures in layered, transition metal dihalides and trihalides *Crystals* **7** 121
[19] Manser J S, Christians J A and Kamat P V 2016 Intriguing optoelectronic properties of metal halide perovskites *Chem. Rev.* **116** 12956–3008
[20] Leo K 2015 Perovskite photovoltaics: signs of stability *Nat. Nanotechnol.* **10** 574–5
[21] Wang G *et al* 2015 Wafer-scale growth of large arrays of perovskite microplate crystals for functional electronics and optoelectronics *Sci. Adv.* **1** e1500613
[22] Calabrese J, Jones N, Harlow R, Herron N, Thorn D and Wang Y 1991 Preparation and characterization of layered lead halide compounds *J. Am. Chem. Soc.* **113** 2328–30
[23] Zhu X, Wangyang P, Sun H, Yang D, Gao X and Tian H 2016 Facile growth and characterization of freestanding single crystal PbI_2 film *Mater. Lett.* **180** 59–62
[24] Zhong M, Huang L, Deng H-X, Wang X, Li B, Wei Z and Li J 2016 Flexible photodetectors based on phase dependent PbI_2 single crystals *J. Mater. Chem.* C **4** 6492–9
[25] Shah K, Olschner F, Moy L, Bennett P, Misra M, Zhang J, Squillante M and Lund J 1996 Lead iodide x-ray detection systems *Nucl. Instrum. Methods Phys. Res.* A **380** 266–70
[26] Bacaksiz C and Sahin H 2016 Single layer PbI_2: hydrogenation-driven reconstructions *RSC Adv.* **6** 89708–14
[27] Zhong M, Zhang S, Huang L, You J, Wei Z, Liu X and Li J 2017 Large-scale 2D PbI_2 monolayers: experimental realization and their indirect band-gap related properties *Nanoscale* **9** 3736–41
[28] Clever H L and Johnston F J 1980 The solubility of some sparingly soluble lead salts: an evaluation of the solubility in water and aqueous electrolyte solution *J. Phys. Chem. Ref. Data* **9** 751–84
[29] Patnaik P 2003 *Handbook of Inorganic Chemicals* vol 529 (New York: McGraw-Hill)
[30] Castellanos-Gomez A, Buscema M, Molenaar R, Singh V, Janssen L, van der Zant H S and Steele G A 2014 Deterministic transfer of two-dimensional materials by all-dry viscoelastic stamping *2D Mater.* **1** 011002
[31] Baibarac M, Preda N, Mihut L, Baltog I, Lefrant S and Mevellec J 2004 On the optical properties of micro-and nanometric size PbI_2 particles *J. Phys.: Condens. Matter* **16** 2345
[32] Kariper İ 2016 Optical and structural properties of PbI_2 thin film produced via chemical dipping method *Opt. Rev.* **23** 401–8
[33] Castellanos-Gomez A, Navarro-Moratalla E, Mokry G, Quereda J, Pinilla-Cienfuegos E, Agraït N, van der Zant H S, Coronado E, Steele G A and Rubio-Bollinger G 2013 Fast and reliable identification of atomically thin layers of $TaSe_2$ crystals *Nano Res.* **6** 191–9
[34] Frisenda R *et al* 2017 Micro-reflectance and transmittance spectroscopy: a versatile and powerful tool to characterize 2D materials *J. Phys. D: Appl. Phys.* **50** 074002
[35] Ghasemi F, Frisenda R, Dumcenco D, Kis A, Perez de Lara D and Castellanos-Gomez A 2017 High throughput characterization of epitaxially grown single-layer MoS_2 *Electronics* **6** 28
[36] Graf D, Molitor F, Ensslin K, Stampfer C, Jungen A, Hierold C and Wirtz L 2007 Spatially resolved Raman spectroscopy of single- and few-layer graphene *Nano Lett.* **7** 238–42
[37] Lee C, Yan H, Brus L E, Heinz T F, Hone J and Ryu S 2010 Anomalous lattice vibrations of single- and few-layer MoS_2 *ACS Nano* **4** 2695–700
[38] Ledinský M, Löper P, Niesen B, Holovský J, Moon S-J, Yum J-H, De Wolf S, Fejfar A and Ballif C 2015 Raman spectroscopy of organic–inorganic halide perovskites *J. Phys. Chem. Lett.* **6** 401–6
[39] Wangyang P, Sun H, Zhu X, Yang D and Gao X 2016 Mechanical exfoliation and Raman spectra of ultrathin PbI_2 single crystal *Mater. Lett.* **168** 68–71
[40] Condeles J F, Ando R A and Mulato M 2008 Optical and structural properties of PbI_2 thin films *J. Mater. Sci.* **43** 525–9

[41] Grisel A and Schmid P 1976 Polytypism and lattice vibrations of PbI_2 *Phys. Status Solidi* b **73** 587–91
[42] Preda N, Mihut L, Baibarac M, Baltog I and Lefrant S 2006 A distinctive signature in the Raman and photoluminescence spectra of intercalated PbI_2 *J. Phys.: Condens. Matter* **18** 8899
[43] Zhou M, Duan W, Chen Y and Du A 2015 Single layer lead iodide: computational exploration of structural, electronic and optical properties, strain induced band modulation and the role of spin–orbital-coupling *Nanoscale* **7** 15168–74
[44] Warren R and Liang W 1993 Raman spectroscopy of new lead iodide intercalation compounds *J. Phys.: Condens. Matter* **5** 6407
[45] Plechinger G, Mann J, Preciado E, Barroso D, Nguyen A, Eroms J, Schueller C, Bartels L and Korn T 2014 A direct comparison of CVD-grown and exfoliated MoS_2 using optical spectroscopy *Semicond. Sci. Technol.* **29** 064008
[46] Liu X, Ha S T, Zhang Q, de la Mata M, Magen C, Arbiol J, Sum T C and Xiong Q 2015 Whispering gallery mode lasing from hexagonal shaped layered lead iodide crystals *ACS Nano* **9** 687–95
[47] Aslani A, Arefi M, Beyki-Shuraki K and Babapoor A 2013 Direct syntheses, characterization and optical analysis of PbX_2 (X = I, Br and Cl) nanoparticles without any additives *J. Saudi Chem. Soc.* **17** 403–7
[48] Schmidt T, Lischka K and Zulehner W 1992 Excitation-power dependence of the near-band-edge photoluminescence of semiconductors *Phys. Rev.* B **45** 8989–94
[49] Tongay S, Suh J, Ataca C, Fan W, Luce A, Kang J S, Liu J, Ko C, Raghunathanan R and Zhou J 2013 Defects activated photoluminescence in two-dimensional semiconductors: interplay between bound, charged, and free excitons *Sci. Rep.* **3** 2657
[50] Klee V, Preciado E, Barroso D, Nguyen A E, Lee C, Erickson K J, Triplett M, Davis B, Lu I-H and Bobek S 2015 Superlinear composition-dependent photocurrent in CVD-grown monolayer $MoS_{2(1-x)}$ Se_{2x} alloy devices *Nano Lett.* **15** 2612–9
[51] Furchi M M, Polyushkin D K, Pospischil A and Mueller T 2014 Mechanisms of photoconductivity in atomically thin MoS_2 *Nano Lett.* **14** 6165–70
[52] Island J O, Blanter S I, Buscema M, van der Zant H S J and Castellanos-Gomez A 2015 Gate controlled photocurrent generation mechanisms in high-gain In_2Se_3 phototransistors *Nano Lett.* **15** 7853–8